Received: 12 March 2021 | Accepted: 13 March 2021

DOI: 10.1002/mdp2.222

REPORT

WILEY

A non-crimp fabric mechanical characterization for the production of aerospace components

Marcello A. Lepore | **Luca Ferrante** | **Luigi Sanguigno** | **Angelo R. Maligno**

Institute for Innovation in Sustainable Engineering, University of Derby, Derby, UK

Correspondence
Marcello A. Lepore, Institute for Innovation in Sustainable Engineering, University of Derby, Quaker Way, Derby DE1 3HD, UK.
Email: m.lepore@derby.ac.uk

Funding information
Clean Sky 2 Joint Undertaking, Grant/Award Number: 831955

Abstract

This work shows a procedure for the mechanical characterization of a new composite for aerospace. Initially, a preliminary test campaign has been carried out to identify the most suitable fabric and resin for the production of the new composite. Subsequently, the production of the composite plaques has been planned. Then, plaques with different orientation of the layers and thicknesses have been obtained. From each of these plaques' coupons for the experimental tests, needed to the mechanical characterization of the composite, have been obtained. The experimental tests have been carried out in a certified laboratory with electromechanical machines and according to ASTM standards. For each experimental test, the trend of the stress–strain curves has shown a typical behavior up to failure. An analysis of the coefficient of variation, based on the statistical mean of parameters calculated with the experimental tests, has been carried out to evaluate the reproducibility of the tests in different laboratories.

KEYWORDS

carbon/epoxy, composites, delamination, mechanical properties, mechanical testing

1 | INTRODUCTION

The aerospace industry is one of the key sectors that has driven the growth in the use of composite materials in recent years, thanks to large manufacturers attracted by the considerable potential for reducing fuel consumption and carbon dioxide emissions. Indeed, despite being more expensive than traditional metallic materials, composites now reach a higher strength, allowing to reduce the weight of the aircraft, the cost of fuel per passenger transported, and ultimately representing an economic advantage. It should also be underlined how these materials also provide greater fatigue resistance in repeated take-off/landing operations than metals, causing a reduction in the frequency of inspections required throughout the life of the aircraft and in maintenance costs.[1] Other advantages presented by reinforced polymers, such as high corrosion resistance, low dielectric loss in radar transparency, capability to form in large critical shapes in less manufacturing time reducing number of parts required, and assembly times.[2] The idea behind composite materials is to combine mechanical properties found separately in two or more different materials in a single material. The combination of the phases gives rise to a new material that highlights the best characteristics of the two components. Of the two phases, one is the reinforcement, and the other is the matrix. Epoxy resins are the most widely used

for aeronautical structures made to date as they have good mechanical properties and excellent resistance to chemical agents. Furthermore, being a thermosetting resin, it has higher operating temperatures than those of thermoplastics. Carbon fiber is the most used fiber in the aeronautical field due to its stiffness and resistance combined with a low specific weight. The most traditional method for the production of complex parts is to use unidirectional fiber prepreg tapes arranged in a suitable lay-up in a mold and cured in an autoclave. This process has been successful and widespread until now in the aerospace industry. However, this manufacturing system represents one of the most important cost items in the production of components in composite materials. In addition, the prepreg materials are expensive and require storage in freezers and accurate control of exposure times at room temperature. As the aerospace industry moves to consider more and more structural parts for larger transport aircraft, alternative and cheaper manufacturing approaches are increasingly sought for commercial airliners. Therefore, interest has increased in the use of dry fabrics that allow the construction of preforms of varying complexity coupled with manufacturing based on liquid composite molding (LCM) methods. Liquid composite molding consists of a variety of composite manufacturing processes where the liquid state matrix material (e.g., epoxy resin) is forced into the dry reinforced reinforcing material (e.g., carbon fiber fabric). LCM methods comprise resin transfer molding (RTM), vacuum-assisted RTM (VARTM), and injection compression molding (ICM).[3] The main goal is to achieve complete impregnation as the resin flows between the bundles of fibers. In the case of the RTM positive operating pressures are used, while in the vacuum infusion, the pressure is lower than atmospheric pressure. Instead, VARTM uses a process that operates with positive injection pressures, while the mold cavity is under vacuum conditions. Positive operating pressure techniques require matched molding (two or more-part molds), while vacuum infusion is usually done using a flexible membrane (e.g., polymer foil) on the mold. RTM and VRTM also differ in the type of molds used, while the former uses a mold and counter-mold system, the latter is usually performed using a flexible membrane (such as a polymer) on the mold.[4] Dry reinforcements offer significant advantages over prepreg materials such as lower prices, longer shelf-life, and above all the ability to avoid the expensive autoclave hardening process. One of the most attractive composite material forms that has evolved from the textile industry is that of multiaxial non-crimp fabrics (NCF). These materials are made up of layers of what are actually unidirectional layers arranged in a number of possible orientations with respect to the warp direction of the fabric, with the fabric itself created by a stitching process connecting the bundles in each layer. Unlike the woven tow systems, NCF lack of gross crimp, but they inevitably have some waviness in the plane of the fabric. However, the effect of this slight waviness is negligible on the in-plane elastic and strength properties if compared with unidirectional reinforcement.[5,6] The major advantage of NCFs over unidirectional is that the combination of multiple layers of fibers, stacked in a single reinforcement system, leads to a faster and cheaper preform production process as the lay-up takes place on a single axis.[7] The advantage is even greater when using automated fiber lay-up devices such as dry automated fiber placement (DAFP).[8] After all, the importance acquired by the NCF is highlighted by the various researches conducted in recent years regarding the composites made using this type of reinforcement. Since the nineties, research on non-crimped reinforcements have focused on the different aspects of this type of reinforcement. Hogg et al. explored the mechanical properties of NCF biaxial and quadriaxial as a function of aerial weight[9] whereas Bibo et al. focused on the comparison between non-crimped fabric and unidirectional composites.[10] Lomov has made a fundamental contribution to the understanding, design, and implementation of the NCF.[11–14] Damage on non-crimp fabrics composites loaded in tension has been investigated by Edgren.[15] The damage mechanism has also been studied for non-crimp laminates subject to fatigue using digital image correlation[16] and for bolted joint NCF both experimentally and by FE modelling.[17,18] Moreover, compression on quasi-isotropic NCF laminates as a function of the stacking sequence[19] and as a function of waviness on unidirectional NCF[20] has been investigated. Some authors extended the characterization to more complex stress types, considering combinations of compressive and shear loads.[21] Vallons et al. investigated the dependence of stiffness, strength, and fatigue life from off-axis loads.[22] The Mode I delamination has been also studied, considering the effect of reinforcement through thickness.[23] Some authors explored the response to the shear stress[24,25] for dry non-crimp fabrics. The study of NCF composites also concerned the effects of the presence or absence of notches on laminates subjected to tensile and compression tests.[26] Finally, impact response of carbon/epoxy NCF laminates has been studied, comparing its properties to the properties of woven fabric laminates.[27] The need to improve the impact response has also led to the creation of hybrid non-crimp fabric laminates with glass, carbon, and polypropylene fibers.[28–30] An important aspect to take into account when using composite materials for structural uses is that of the effects that environmental conditions can have on its performance. Since the stiffness and strength of a composite material decrease with increasing temperature and moisture content, their evaluation is important in structural applications. The weak point of the response of composite materials to increasing temperature is given by the resin of the matrix. When heated to mild temperatures, fiber-reinforced plastics soften and creep, causing a significant decrease in both

strength and stiffness.[31] This occurs at a temperature referred to as the glass transition temperature, T_g. Above T_g, the elastic modulus of a polymer is significantly reduced due to changes in its molecular structure. The range of glass transition temperature is in the range of 65–120°C, within which the resin changes from glassy state to rubbery state.[32] As a result of the softening of the resin, there is first of all a reduction in the strength of the resin itself, followed by a weakening of the binding effect of the fibers, with a consequent rapid reduction in the strength of the fiber-reinforced composites. However, fibers have better thermal properties than resin, so they can continue to carry a certain load if aligned in appropriate directions. On the other hand, the overall properties of the composite are reduced due to a reduction in force transfer between the fibers through adhesion to the resin.[33] The importance of the temperature effect is at the origin of several studies on the response to quasi-static loads on composite materials reinforced with carbon fiber.[34–36] This work is part of a larger research project aimed to extend the use of NCF carbon/epoxy composite materials to the creation of aircraft parts that are traditionally made of metal such as the landing gear, thus obtaining advantage in terms of both weight reduction, mechanical properties, and cost reduction. For this reason, an experimental campaign has been carried out in order to characterize in the most exhaustive way epoxy composite laminates whose reinforcement is an innovative quasi-unidirectional dry hybrid NCF, made of carbon and glass fibers. In this type of NCF, the carbon is the reinforcement part that supports most of the load and disposed in a unidirectional-like way. The glass fiber is instead arranged according to three different directions, and its main task is to contribute, together with the stitching, to keep the carbon fiber in position during the impregnation process via RTM. Samples with different lay-ups have been made according to the type of test to be performed in accordance with ASTM standards.

2 | MATERIALS AND METHODS

2.1 | Materials

2.1.1 | Non-crimp fabric

A quasi-unidirectional (QU) composite material and a specific resin have been chosen to be used with resin transfer molding (RTM) process. Then, the U-C-298 g/m^2-1270 mm SAERTEX crimp-free fabric with a very high modulus and strength has been selected. The fabric construction has been reported in Table 1.

2.1.2 | Epoxy resin

An epoxy resin for high performance matrix polymers and for advanced composites has been used.

The adopted two components epoxy resin is

- BDP 4294 (epoxy resin).
- CURAMINE 32-494 (curing agent).

The cure schedule is 24 h at 25°C + 1 h at 120°C + 2 h at 180°C. The values of compression modulus and strength of the cured resin are not included in the specimens manufacture; thus, these properties have been estimated as well through experimental tests and reported in Table 2 in order to complete the resin specifications. Experimental tests have been carried out on samples of the epoxy resin cured at the same cure conditions described in the manufacturer's

TABLE 1 7001549/SAERTEX article construction data

Layer	Construction	Areal weight (g/m^2)	Tolerance	Material
4	90°	8	±5.0%	E-glass 68 TEX
3	0°	274	±5.0%	Teijin Carbon Japan IMS60 E13 24K
2	60°	6	±5.0%	E-glass 68 TEX
1	−60°	6	±5.0%	E-glass 68 TEX

Property	Typical result
T_g	204°C
Tensile strength	90 N/mm^2
Tensile modulus	2900 N/mm^2
Compressive strength	59 N/mm^2
Compressive modulus	2743 N/mm^2
Elongation at break	4%
Flexural strength	85 N/mm^2
Water absorption	0.55%

TABLE 2 Properties and typical results of BDP 4294 cured with Curamine 32-494

TABLE 3 Test matrix at room temperature (preliminary tests have been marked in red color)

Test type (outcome)	Test condition	Test orientation	Standard	Minimum no. of coupons
%VOID and FVF	-	-	ASTM D3171	6
DMA (T_g)	-	-	ASTM D7028	5
Standard tension (modulus/strength/Poisson)	RT	0°	ASTM D3039M	5
		90°	ASTM D3039M	5
Standard compression (modulus/strength/Poisson)	RT	0°	ASTM D6641	5
		90°	ASTM D6641	5
In-plane shear (shear modulus and strength)	RT	±45°	ASTM D3518M	5
ILSS (apparent interlaminar shear strength)	RT	0°	EN2563	5
Open hole tension (tensile strength)	RT	0°	ASTM D5766	5
Open hole compression (compressive strength)	RT	0°	ASTM D6484	5

schedule. Then, five small cylindrical samples of cured epoxy resin have been tested at room temperature to provide compressive strength and modulus of the cured resin.

2.2 | Methods

To characterize the behavior at room temperature of the composite material, several standard experimental tests have been performed. These experimental tests allowed to know the material properties like void percent (% Void) and fiber volume fraction (FVF) that can be used for creating the lamina model by means of micromechanical approach by commercial software. The glass transition temperature (T_g) of the cured resin, specified by the manufacturer and reported in Table 2, could be different from that obtained by dynamic mechanical analysis (DMA) testing a composite specimen. For this reason, DMA tests have been performed at room temperature on composite samples. Important tests such as the dynamic mechanical analysis (DMA), in-plane shear (IPS), the standard tensile and compression tests, and the interlaminar shear strength (ILSS) have been performed. The DMA tests have provided the glass transition temperature (T_g) of the composite (critical temperature) while the both tensile and compressive standard tests have provided longitudinal modules, ultimate strength, and Poisson's ratio. The IPS tests have provide the shear modulus and shear strength, respectively, while the ILSS tests have been necessary to know the apparent interlaminar shear strength (tau) and therefore to understand this mode of failure. Table 3 shows the types of tests carried out and necessary to characterize the composite at room temperature, with relative standards and number of specimens to be tested. The orientation of the carbon fibers has been indicated in decimal degrees where 0° refers to the carbon fibers oriented in the direction of the applied load.

Preliminary tests on specimens of composite materials like %VOID and FVF, DMA (T_g), have been carried out as expected in Table 3 (highlighted in red color). Initially, attention will be paid to the estimate of the %Void and FVF. It is worth noting that void volume of a composite material may significantly affect some of its mechanical properties. Moreover, higher void volumes usually mean lower fatigue resistance, greater susceptibility to moisture penetration and weathering, and increased variation or scatter in strength properties. Knowledge of the void volume percent of a composite material is desirable as an indication of the quality of a composite. Moreover, reinforcement content (FVF) may be used to normalize mechanical properties affected by amount of reinforcement in the coupon. Regarding the DMA is a test method that covers the procedure for the determination of the dry or wet (moisture conditioned) glass transition temperature (T_g) of polymer matrix composites containing high-modulus (20 GPa) fibers under flexural oscillation mode, which is a specific subset of the DMA method. However, the T_g is dependent upon the physical property measured, the type of measuring apparatus, and the experimental parameters used.

Table 4 shows the outcomes of the experimental tests reported in Table 3. The standard tension, E_{11}, indicates the Young's modulus, and ν_{12} and ν_{13} are the Poisson's ratios, while S_1 is the ultimate strength. At 90°, E_{22}, modulus, the Poisson's ratio, ν_{23}, and the ultimate strength, S_2, are calculated. The ±45° in-plane shear tests provide the shear modules, G_{12}, and the ultimate shear strength, S_{12}. The out-of-plane shear module, G_{13}, has been chosen equal to G_{23}. G_{13} is calculated with the formula, $G_{13} = \alpha\ G_{12}$, where α is a coefficient equal to 0.58 for carbon/epoxy laminates with low carbon fibers. The ultimate strength, $-S_1$ and $-S_2$, has been obtained with standard compression tests at 0° and 90°, respectively.

2.2.1 | Plan for plaques manufacturing

The coupons necessary to carry out the mechanical tests have been obtained from plaques of composite with layouts and thicknesses defined in a plaques production plan. ASTM standards required different thicknesses and layouts for different mechanical tests. In Table 5, the type of lay-up and number of plies have been reported as required by the plaques production plan.

TABLE 4 Outcomes provided by test matrix at room temperature

Test type	Test condition	Test orientation	Outcome
Standard tension (modulus/strength/Poisson)	RT	0°	E_{11}, ν_{12}, ν_{13}, S_1
		90°	E_{22}, ν_{23}, S_2
Standard compression (modulus/strength/Poisson)	RT	0°	E_{11}, ν_{12}, $-S_1$
		90°	E_{22}, ν_{12}, $-S_2$
In-plane shear (shear modulus and strength)	RT	±45°	G_{12}, S_{12}
ILSS (apparent interlaminar shear strength)	RT	0°	τ (MPa)

TABLE 5 Number of plaques and plies

Plaque ID	Number of plies
P-001	8 plies, unidirectional [0°]
P-002	
P-003	8 plies, bidirectional [0°/90°]
P-004	
P-005A	12 plies, unidirectional [0°]
P-005B	
P-006	12 plies, bidirectional [0°/90°]
P-007	
P-008	

2.2.2 | Plan for coupons manufacturing

Coupons have been manufactured according to the quality standard required by the aeronautical sector about resin transfer molding (RTM) technology. It has been estimated an overall number of eight plaques of composite to be produced with RTM process. Following a cutting plan, several specimens have been obtained. Therefore, four plaques of composite have been produced with a thickness of 2.5 ± 3% mm while other four plaques have been produced with a thickness of 3.6 ± 3% mm. This is because the planned tests require that specimens with different thickness values be tested (see Table 6). Table 6 shows some information on test types and on the relative number of plies and thicknesses.

It is worth noting that ply scheme of bidirectional composite is balanced and symmetric. This configuration has been adopted to produce specimens for the in-plane shear. The conventional bidirectional composite scheme has been reported in that follows,

- One plaque with eight plies of carbon fiber, with the following lay-up, [0/0/0/0] s
- Three plaques with eight plies of carbon fiber, with the following lay-up, [0/90/0/90/0/90] s.
- One plaque with 12 plies of carbon fiber, with the following lay-up, [0/0/0/0] s
- Three plaques with 12 plies of carbon fiber, with the following lay-up, [0/90/0/90/0/90] s

Laminates consisting of Saertex IMS60/Epoxy Bitrez and BDP 4294–Curamine 32-494 have been used for mechanical testing.

3 | RESULTS AND DISCUSSION

All static tests have been performed with Shimadzu and Instron electromechanical testing machines with load cells between 50 kN and 250 kN. All DMA tests have been carried out using a TA Instruments Q800 dynamic mechanical analyzer. All tensile, compression, and IPS specimens have been strain gauged with Vishay Measurements Group Tee Rosette, with 350 ohms of grid resistance and gauge factor 2.1. All the failure mode symbols shown in the following tables can be found in the corresponding ASTM standards.

3.1 | Plaques manufacturing

RTM tool used vacuum to hold the lid shut; it also had four small toggle clamps on the outside to support the glass lid. Full vacuum on the flange and tool cavity has been obtained. The mold thickness has been set to 2.8 mm for the 8-ply plaques and 4.2 mm for the 12-ply plaques. The epoxy resin and hardener have been preheated to 40°C. Once mixed, they are placed in a heated pressure pot at 35°C. The tool surfaces have been heated to 35°C. The average time taken for the resin to fill the mold has been ∼110 min, and this is quite close to the gel time of the resin at 35°C. Considering the unidirectional plaques, the filled has been obtained through one edge of the lay-up that allowed the resin to travel along the length of the fibers. Some difficulties occurred getting the resin to travel more than 200 mm along the length of fibers. Full vacuum pressure and 1.0-bar injection pressure have been used. Increasing the injection pressure leaded to fiber wash (due to the reduced fiber volume fraction) and bowing of the mold top surface. For the bidirectional plaques, the filling of the mould has been obtained through one edge injection, and the resin has been infused from the outside to the center point. An injection pressure as well as the vacuum pressure to ensure the resin travelled all the way to the center of the plaque has been used. As with the unidirectional plaques, 1.0-bar injection pressure has been

TABLE 6 Information on the number of plaques with relative thickness, number of plies, and ASTM standards

Standard	Test type	No. of plies	Thickness (mm)	No. of plaques
ASTM D3039M	Standard tension	8	2.5 ± 3%	1
ASTM D3518M	In-plane shear (IPS)	8	2.5 ± 3%	1
ASTM D6641	Standard compression	12	3.6 ± 3%	1
EN2563	ILSS	12	3.6 ± 3%	1

used. It is worth noting that to use a higher pressure and higher volume fraction to get the resin to infuse through the fiber without washing the fibers has been not possible. Eight-ply plaques with nominal thickness of 2.4 mm and an average thickness of 3.03 mm for 12-ply plaques have been observed (Figure 1).

The Saertex fiber seemed to have very low permeability in all three directions. It has been difficult to get the resin to travel more than 200 mm in the *x*/*y* direction. To do this required increasing positive injection pressure, which caused issues as the fiber washed inwards and became wavy. The pressure also caused the glass lid to flex upwards, which further reduced the compression on the fibers and increased waviness. It has been also attempted center point injection; however, the *z* direction permeability seemed very low. The resin only infused ∼30 mm from the injection point even with ∼3-bar injection pressure. This low *z* direction permeability also explained why the vacuum level seemed to have a low impact on the infusion performance, probably the fabric "sealed" the vacuum port off.

3.2 | Test specimen manufacture

Test specimens have been cut from the laminates using a composite plate saw fitted with a diamond metal bonded cutting disc. All specimens have been cut to the dimensions and tolerances stated in the standards. Areas to be bonded with end tabs have been prepared by wet blasting using a vac blaster containing 180- to 220-μm aluminum oxide to achieve a water break-free surface. After preparation, the surfaces have been then washed and dried. Immediately, prior to bonding, the prepared surfaces have been wiped with a solvent to remove any remaining contaminants. Then, a 2-mm-thick woven glass epoxy has been used for end-tabbing. Bonding of end tabs to the test specimens has been done using a film adhesive cured for a minimum of 2 h at 100°C with pressure applied. Tensile and IPS specimen widths and thicknesses have been measured in three locations along the gauge length with the average used in all calculations. Compression and ILSS test specimens have been measured for their width and thickness once at the center of the gauge length. The machines used to carry out the static tests have been electro-mechanical test machines calibrated to ISO 7500-1 and ASTM E4-16. The static tests have been performed as required by the test plan.

3.3 | Static tests

3.3.1 | ASTM D3039 UD tensile

All testing have been performed using equipment and methods that comply with the requirements of ASTM D3039. Testing has been performed at a constant crosshead extension of 2 mm/min. Properties calculated include tensile modulus E_{11} and E_{22}, ultimate tensile strength, and Poisson's ratio. The tensile modulus and Poisson's ratio have been calculated from the stress strain curve between 1000 usn and 3000 usn axial strain. In Table 6, details of the test results for 0° UD tensile testing have been shown. The values of SD/average represent the coefficient of variation and provide a tool to compare quickly different data series. Anyway, the average 0° UD tensile strength has been found to be 1293.03 MPa with a coefficient of variation (C of V) of 6.98%. The average tensile modulus has been found to be 97.20GPa with a C of V of 2.14%.

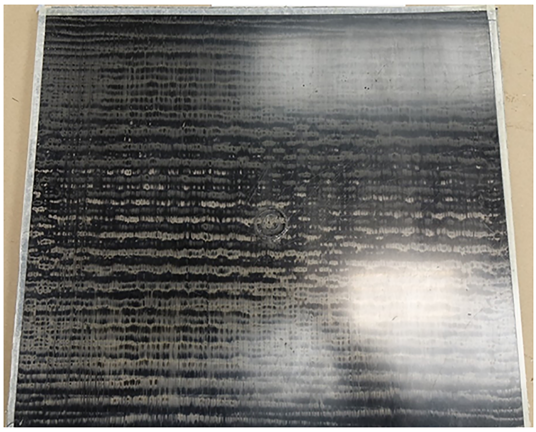

FIGURE 1 Eight-ply plaque after curing

Average strain at failure has been 12,207 usn (C of V 6.61%), and all specimens displayed explosive failures within the gauge length. The 0° tensile failure modes are reported in Table 7 as well. Characters XGV are for eXplosive Gauge Various and are reported in ASTM D3039. In Figure 2, both test machine and the specimen have been shown.

In Table 8, details of test results for the 90° UD tensile testing have been reported.

The average 90° UD tensile strength has been found to be 31.70 MPa with a C of V of 8.59%. The average tensile modulus has been 7.24 GPa with a C of V of 3.11% while the average strain at failure has been 4370 usn (C of V 8.62%) and all specimens displayed lateral failure modes within the gauge length. Furthermore, a typical plot of the stress–strain response as measured by the strain gauges has been obtained. Characters LGT and LGB are for lateral gauge top and lateral gauge bottom, respectively, and are reported in ASTM D3039. In Figure 3, the failure modes of tested specimens have been shown.

3.3.2 | ASTM D6641 UD compression

All testing have been performed using equipment and method that complies with the requirements of ASTM D6641. A test fixtures combined loading compression fixture has been used to perform the testing with specimens

TABLE 7 Test results for 0° UD tensile testing

0° tensile unaged tested at RT							
Specimen ID	**Width (mm)**	**Thickness (mm)**	**0° tensile strength (MPa)**	**0° tensile modulus (GPa)**	**Strain at failure (usn)**	**Poisson's ratio**	**Failure mode**
SPECIMEN-1	15.12	3.28	1352.19	98.54	12,069	0.31	XGV
SPECIMEN-2	15.04	3.33	1313.23	99.55	12,479	0.37	XGV
SPECIMEN-3	15.03	3.38	1192.24	97.74	11,496	0.37	XGV
SPECIMEN-4	15.10	3.41	1208.04	94.47	11,535	0.36	XGV
SPECIMEN-5	15.05	3.46	1399.45	95.72	13,455	0.35	XGV
Average	15.07	3.37	1293.03	97.20	12,207	0.35	
SD	0.04	0.07	90.30	2.08	807.35	0.03	
C of V (%)	0.27	2.12	6.98	2.14	6.61	7.22	

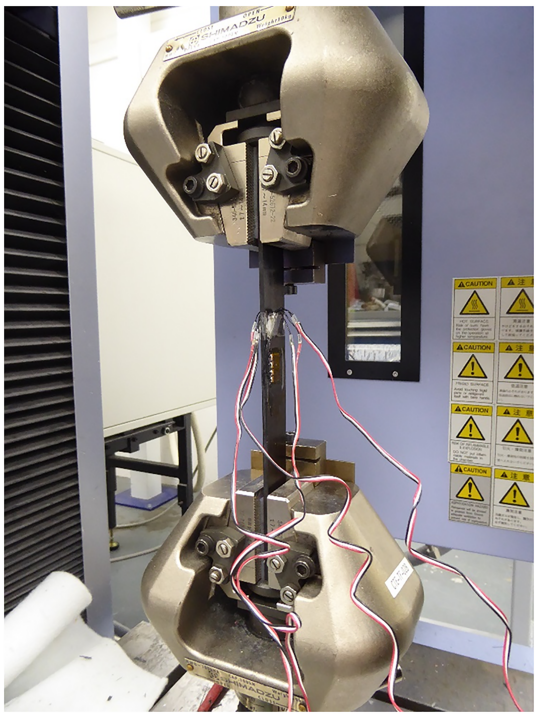

FIGURE 2 Tensile test (testing machine and specimen)

TABLE 8 Test results for 90° UD tensile testing

90° tensile unaged tested at RT							
Specimen ID	**Width (mm)**	**Thickness (mm)**	**0° tensile strength (MPa)**	**0° tensile modulus (GPa)**	**Strain at failure (usn)**	**Poisson's ratio**	**Failure mode**
SPECIMEN-1	25.17	3.07	36.06	7.57	4,804	0.03	LGT
SPECIMEN-2	25.09	3.24	29.68	7.21	4,107	0.03	LGB
SPECIMEN-3	25.10	3.35	31.54	7.20	4,413	0.03	LGT
SPECIMEN-4	25.09	3.42	29.17	7.25	3,885	0.03	LGB
SPECIMEN-5	25.13	3.55	32.04	6.94	4,642	0.04	LGT
Average	25.12	3.32	31.70	7.24	4370	0.03	
SD	0.04	0.18	2.72	0.22	376.77	0.00	
C of V (%)	0.14	5.51	8.59	3.11	8.62	11.27	

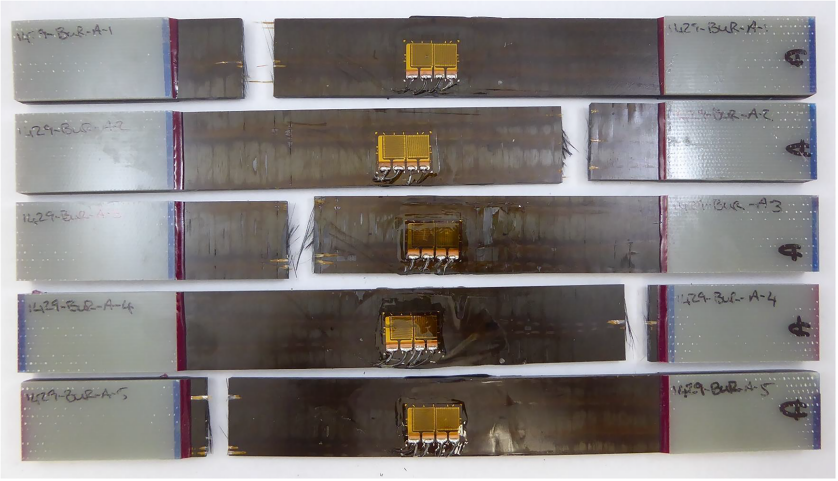

FIGURE 3 Tensile failure modes (90°)

loaded via end and shear loading. Testing has been performed at a constant crosshead speed of 1.3 mm/min. The compressive modulus E_{11} and E_{22} has been obtained from the gradient of the constructed compression stress versus compression strain curve between 1000 usn and 3000 usn strain values. All compression tests have been checked for signs of bending. The specimens have been checked using the following bending criteria, $|-\varepsilon_{11b}-\varepsilon_{11a}\varepsilon_{11b}+\varepsilon_{11a}| \leq 0.1$, where ε_{11a} and ε_{11b} (or ε_{22a} and ε_{22b}) are the longitudinal strains on opposite faces of the specimen. Table 9 details the test results of the 0° UD compression testing. A typical plot of the stress–strain response as measured by the strain gauges has been observed. The 0° compressive failure modes can be seen in ASTM D6641.

The average 0° compression strength has been found to be 909.66 MPa with a C of V of 5.45%. The average compressive modulus has been 116.35 GPa with a C of V of 3.07%. The average failure strain has been found to be 8264 usn (C of V 4.48%), where four of six specimens tested failed via through thickness shear failure modes and two specimens failed via end crushing. End crushing is typically an invalid failure mode; however, the results have been retained for calculating the average strengths as they are typically conservative values and fall within the spread of results of the four specimens with valid failure modes. Table 10 details the test results of the 90° UD compression testing. A typical plot of the stress–strain response as measured by the strain gauges has been observed. Characters HAT are for through thickness at grip top, characters HGB are for through thickness at gauge bottom, and characters HAB are for through thickness at grip bottom.

The 90° compressive failure modes can be seen in Figure 4.

TABLE 9 Test results for 0° UD compression testing

0° compression unaged tested at RT							
Specimen ID	**Width (mm)**	**Thickness (mm)**	**0° compression strength (MPa)**	**0° compression modulus (GPa)**	**Poisson's ratio**	**Failure strain (usn)**	**Failure mode**
SPECIMEN-1	12.80	3.77	979.83	117.85	−0.35	8837	HAT
SPECIMEN-2	12.79	3.78	953.78	120.07	−0.38	8371	End C.
SPECIMEN-3	12.80	3.79	920.97	118.55	−0.34	8085	End C.
SPECIMEN-4	12.81	3.81	865.73	113.78	−0.23	7854	HGB
SPECIMEN-5	12.79	3.83	871.28	111.51	−0.43	8175	HAB
Average	12.80	3.79	909.66	116.35	−0.35	8264.0	
SD	0.01	0.02	49.54	3.57	0.07	370.05	
C of V (%)	0.08	0.62	5.45	3.07	−20.64	4.48	

TABLE 10 Test results for 90° UD compression testing

90° compression unaged tested at RT							
Specimen ID	**Width (mm)**	**Thickness (mm)**	**0° compression strength (MPa)**	**0° compression modulus (GPa)**	**Poisson's ratio**	**Failure strain (usn)**	**Failure mode**
SPECIMEN-1	12.73	3.76	210.96	8.48	−0.02	32,499	BGM
SPECIMEN-2	12.81	3.73	202.58	9.28	−0.03	26,466	BGM
SPECIMEN-3	12.79	3.72	202.73	8.43	−0.02	30,991	BGM
SPECIMEN-4	12.82	3.69	195.53	9.36	−0.03	25,904	BGM
SPECIMEN-5	12.80	3.66	202.34	9.14	−0.02	27,308	BGM
Average	12.79	3.71	202.83	8.94	−0.02	28,634	
SD	0.04	0.04	5.47	0.45	0.00	2932.9	
C of V (%)	0.28	1.03	2.70	4.99	−12.52	10.24	

The average 90° compression strength has been found to be 202.83 MPa with a C of V of 2.70%. The average compressive modulus has been 8.94 GPa with a C of V of 4.99%. The average strain at failure has been 28,634 usn (C of V 10.24%), and all specimens displayed brooming compression failures. Characters BGM are for brooming gauge middle.

3.3.3 | ASTM D3518 in-plane shear

All testing have been performed using equipment and method that has been compliant with the requirements of ASTM D3518. Testing has been performed at a constant crosshead speed of 2 mm/min. The ±45° tensile modulus E_{11} has been obtained from the gradient of the constructed tensile stress versus axial strain curve between 1000 and 3000 usn. The in-plane shear modulus G_{12} has been obtained from the gradient of the constructed shear stress versus shear strain curve between 2000 and 6000 usn shear strain. Additional parameters recorded have been tensile and shear stresses at 5% shear strain, ultimate tensile and shear failure stresses, shear failure strain, and Poisson's ratio (calculated between 1000 and 3000 usn axial strain). Table 11 details the test results of the ±45° in-plane shear (IPS) testing. A typical plot of the tensile stress–strain response as measured by the strain gauges has been found. Characters AGM are for angle gauge middle.

The average tensile and shear strength at failure have been found to be 109.80 MPa and 54.90 MPa, respectively, with a C of V of 1.63%. The tensile modulus has been found to be 8.22 GPa with a C of V of 1.64%, and the shear modulus has been found to be 2.24 GPa with a C of V of 1.32%. The average shear strain at failure has been 50,906 usn (C of

FIGURE 4 Compressive failure modes (90°)

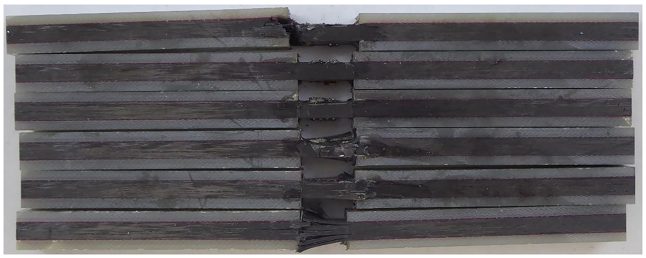

V 8.84%), and all specimens displayed angled failure modes within the gauge length. An example of failure modes can be seen in Figure 5.

While the stress–strain curves relating to the tensile and compression tests show an almost linear trend with often catastrophic failure, the stress–strain curves relating to the IPS tests show progressive and more interesting damaging to show. Thus, in Figure 6, the stress–strain curve for all tested specimen is reported.

3.3.4 | EN 2563 0° biaxial ILSS

All interlaminar shear (ILSS) testing has been performed using equipment and method that has been compliant with the requirements of EN 2563. Testing has been performed with a span to thickness ratio of 5:1 at a constant crosshead speed of 1 mm/min using an ILSS test fixture with 3-mm radius supports and 3-mm radius loading nose. Table 12 details the test results of the 0° biaxial ILSS testing. Example ILS failure modes can be seen in Figure 7.

The average ILS strength has been found to be 38.78 MPa with a C of V of 7.39%.

All specimens displayed valid ILS failure modes. The stress–strain curves relating to the ILLS tests have highlighted progressive damaging and have been shown in Figure 8 for all tested specimens.

3.3.5 | ASTM D7028 DMA

DMA testing has been performed based on the requirements of ASTM D7028 with the following test parameters:

- Clamp: single cantilever
- Frequency: 1 Hz
- Amplitude: 20 μm
- Temperature range: 30–250°C
- Ramp rate: 5°C/min

Properties obtained from these tests have been reported in that follows:

- Onset temperature calculated from the storage modulus curve.
- Glass transition temperature from the loss modulus curve.
- Tan δ temperature.

Anyway, it is worth noting that several factors could affect test results including physical characteristics of the test machine (stiffness, damping, and mass), load accuracy and displacement/strain measurement, loading speed, specimen alignment with applied load, grip parallelism, gripping pressure, and type of load control (displacement, deformation, or load). Additionally, material factors can also affect test results, including material quality, sampling scheme, and sample preparation (dimensional accuracy, tab material, cone, tab adhesive, and so on). Tables 13 and 14 detail the 0°, 90° UD DMA test results, respectively.

The average 0° onset temperature has been 118.75°C with corresponding loss modulus and tan delta values of 155.12°C and 174.47°C. The average 90° onset temperature has been 104.16°C with corresponding loss modulus and tan delta values of 149.49°C and 172.21°C.

TABLE 11 Test results for IPS testing

±45° in-plane shear strength unaged tested at RT											
Specimen ID	**Width (mm)**	**Thickness (mm)**	**Tensile strength @ 5% shear strain (MPa)**	**Shear strength @ 5% shear strain (MPa)**	**Tensile strength @ failure (MPa)**	**Shear strength @ failure (MPa)**	**Tensile modulus (GPa)**	**Shear modulus (GPa)**	**Shear strain at failure (usn)**	**Poisson's ratio**	**Failure mode**
SPEC-1	25.04	3.74	-	-	108.81	54.41	8.38	2.27	47,507	0.82	AGM
SPEC-2	25.04	3.69	110.35	55.17	110.37	55.19	8.21	2.27	54,030	0.77	AGM
SPEC-3	24.93	3.63	-	-	107.57	53.79	8.32	2.24	47,798	0.84	AGM
SPEC-4	25.03	3.76	-	-	109.91	54.96	8.15	2.23	47,892	0.79	AGM
SPEC-5	25.02	3.82	110.99	55.49	112.35	56.18	8.04	2.20	57,304	0.80	AGM
Average	25.01	3.73	110.67	55.33	109.80	54.90	8.22	2.24	50,906	0.80	
SD	0.05	0.07	0.45	0.23	1.79	0.89	0.14	0.03	4499	0.03	
C of V (%)	0.19	1.91	0.41	0.41	1.63	1.63	1.64	1.32	8.84	3.36	

FIGURE 5 Failure mode of IPS test

FIGURE 6 Stress–strain curve of IPS tests

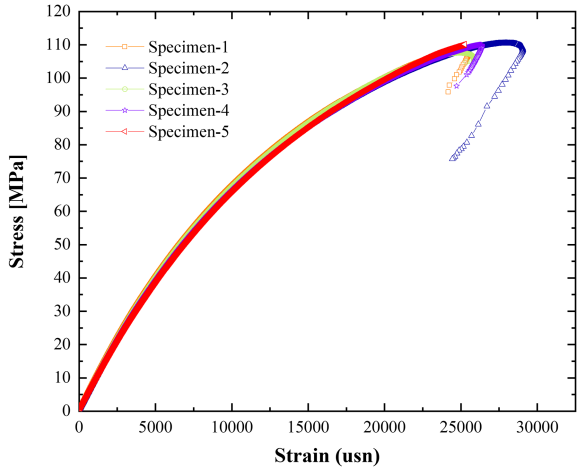

TABLE 12 Test results for ILSS testing

0° ILSS unaged tested at RT				
Specimen ID	**Width (mm)**	**Thickness (mm)**	**ILSS (MPa)**	**Failure mode**
SPECIMEN-1	10.10	4.32	41.33	ILS
SPECIMEN-2	10.10	4.33	37.48	ILS
SPECIMEN-3	10.05	4.33	41.57	ILS
SPECIMEN-4	10.05	4.32	34.67	ILS
SPECIMEN-5	10.10	4.32	38.85	ILS
Average	10.08	4.32	38.78	
SD	0.03	0.01	2.87	
C of V (%)	0.27	0.13	7.39	

FIGURE 7 ILS test failure modes

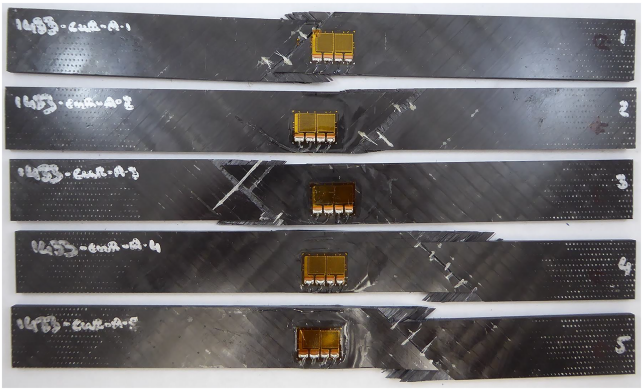

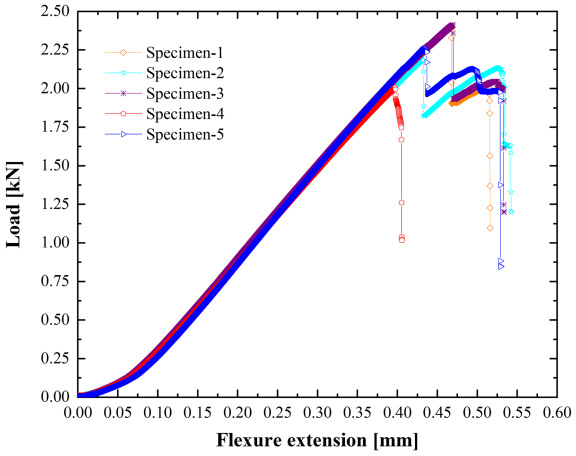

FIGURE 8 Load versus flexure extension of ILSS tests

TABLE 13 Test results for DMA 0° testing

DMA unaged 0°								
Specimen ID	**Width (mm)**	**Thickness (mm)**	**Pretest weight (g)**	**Post-test weight (g)**	**Weight loss (%)**	**Onset temperature °C (storage modulus)**	**T_g temperature °C (loss modulus)**	**Tan delta °C**
Spec-1	10.04	2.77	1.6506	1.6458	0.29%	125.27	156.29	174.06
Spec-2	10.08	3.24	1.8735	1.8669	0.35%	123.01	159.06	177.31
Spec-3	10.10	3.21	1.8633	1.8574	0.32%	116.55	157.33	176.61
Spec-4	10.03	3.61	2.0288	2.0218	0.35%	116.55	153.13	172.42
Spec-5	10.02	3.73	2.0897	2.0821	0.36%	118.50	154.13	172.82
Spec-6	10.06	3.79	2.1221	2.1145	0.36%	112.62	150.76	173.57
Average	10.06	3.39	1.94	1.93	0.34%	118.75	155.12	174.47
SD	0.03	0.39	0.18	0.18	0.03%	4.65	3.02	2.03
C of V (%)	0.31	11.52	9.16	9.13	8.38	3.91	1.95	1.16

TABLE 14 Test results for DMA 90° testing

DMA unaged 90°								
Specimen ID	**Width (mm)**	**Thickness (mm)**	**Pretest weight (g)**	**Post-test weight (g)**	**Weight loss (%)**	**Onset temperature °C (storage modulus)**	**T_g temperature °C (loss modulus)**	**Tan delta °C**
Spec-1	10.09	3.30	1.9065	1.8997	0.36%	102.22	145.39	169.71
Spec-2	10.06	3.77	2.1484	2.1413	0.33%	98.55	141.94	173.96
Spec-3	10.10	3.24	1.8851	1.8772	0.42%	105.41	148.83	169.35
Spec-4	10.18	3.03	1.7906	1.7845	0.34%	110.37	155.19	173.97
Speci-5	10.16	2.91	1.7343	1.7288	0.32%	104.26	156.09	174.04
Spec-6	10.12	3.25	1.8930	1.8863	0.35%	104.16	149.49	172.21
Average	0.05	0.33	0.16	0.16	0.04%	4.34	6.13	2.45
SD	0.50	10.17	8.40	8.40	11.27	4.17	4.10	1.42
C of V (%)	10.09	3.30	1.9065	1.8997	0.36%	102.22	145.39	169.71

4 | CONCLUSIONS

The lightening of structural components of commercial airliners has always aroused much interest in the aeronautical sector. One of the main problems related to the lightening of these parts is related to the mechanical properties of the components that must ensure the necessary strength and safety in operating conditions. The lightening of these structures can make use of carbon fiber composite materials, which, in addition to ensuring a significant reduction in the weight of the structure, can also offer high resistance to the applied loads. The certification process of a new composite material is, however, a very complex activity and requires a large number of tests to produce a statistical analysis capable of providing the correct permissible design. In this perspective, CLEANSKY2/MATRIX is a project that has been created to define a methodology able to reduce the big number of physical tests at basic level (L1) required by a certification test campaign. As part of the matrix project, the constituent materials of the new composite for the aerospace have been identified, and the behavior of the composite material under different load conditions has been evaluated with specific laboratory tests. The statistical investigations carried out on both the results of experimental tests and failure modes have shown their reproducibility in different laboratories according to ASTM standards. The mechanical properties of the composite coupons, obtained from the experimental campaign, have been the starting point for further experimentation needed to identify other important properties such as the fracture toughness and maximum compressive strength after the impact of drop-off laminates.

ACKNOWLEDGMENT

The author would like to acknowledge funding from the Clean Sky 2 Joint Undertaking, project title **"**Improved **M**ethod to **A**nalyse composite materials sui**T**able for SLP structures with the aim of **R**educing the **I**mpact on the required e**X**perimental testing campaign (**MATRIX**)" (project reference no. 831955).

DATA AVAILABILITY STATEMENT

Data generated at a central, large-scale facility, available upon request.

ORCID

Marcello A. Lepore https://orcid.org/0000-0001-6065-1866

REFERENCES

1. Irving P, Soutis C. *Polymer Composites in the Aerospace Industry*. Woodhead Publishing; 2019.
2. Dutton S, Kelly D, Baker A. *Composite Materials for Aircraft Structures*. Seconded. American Institute of Aeronautics and Astronautics; 2004.
3. Advani SG, Sozer EM. Liquid molding of thermoset composites. In: *Comprehensive Composite Materials*. Elsevier; 2000:807-844.
4. Kuentzer N, Simacek P, Advani SG, Walsh S. Correlation of void distribution to VARTM manufacturing techniques. *Compos Part a Appl Sci Manuf*. Mar. 2007;38(3):802-813.
5. Tessitore N, Riccio A. A novel FEM model for biaxial non-crimp fabric composite materials under tension. *Comput Struct*. Jul. 2006;84 (19–20):1200-1207.
6. Petriccione A, Annicchiarico D, Antonucci V, et al. A stiffness volume averaging based approach to model non-crimp fabric reinforced composites. *Compos Sci Technol*. Jan. 2012;72(2):360-369.
7. Bibo GA, Hogg PJ, Backhouse R, Mills A. Carbon-fibre non-crimp fabric laminates for cost-effective damage-tolerant structures. *Compos Sci Technol*. Jan. 1998;58(1):129-143.
8. Veldenz L, Di Francesco, Giddings P, Kim BC, Potter K. Material selection for automated dry fibre placement using the analytical hierarchy process. *Adv Manuf Polym Compos Sci*. Oct. 2018;4(4):83-96.
9. Hogg PJ, Ahmadnia A, Guild FJ. The mechanical properties of non-crimped fabric-based composites. *Composites*. Jul. 1993;24(5): 423-432.
10. Bibo GA, Hogg PJ, Kemp M. Mechanical characterisation of glass- and carbon-fibre-reinforced composites made with non-crimp fabrics. *Compos Sci Technol*. Jan. 1997;57(9–10):1221-1241.
11. Lomov SV, Belov EB, Bischoff T, Ghosh SB, Truong Chi T, Verpoest I. Carbon composites based on multiaxial multiply stitched preforms. Part 1. Geometry of the preform. *Compos Part a Appl Sci Manuf*. Sep. 2002;33(9):1171-1183.
12. Lomov SV, Verpoest I, Barburski M, Laperre J. Carbon composites based on multiaxial multiply stitched preforms. Part 2. KES-F characterisation of the deformability of the preforms at low loads. *Compos Part a Appl Sci Manuf*. Apr. 2003;34(4):359-370.
13. Lomov SV, Barburski M, Stoilova T, et al. Carbon composites based on multiaxial multiply stitched preforms. Part 3: Biaxial tension, picture frame and compression tests of the preforms. *Compos Part a Appl Sci Manuf*. Sep. 2005;36(9):1188-1206.
14. Lomov SV. *Non-Crimp Fabric Composites*. 1st ed. Woodhead Publishing; 2011.

15. Edgren F, Mattsson D, Asp LE, Varna J. Formation of damage and its effects on non-crimp fabric reinforced composites loaded in tension. *Compos. Sci. Technol.* Apr. 2004;64(5):675-692.
16. Nonn S, Kralovec C, Schagerl M. Damage mechanisms under static and fatigue loading at locally compacted regions in a high pressure resin transfer molded carbon fibre non-crimp fabric. *Compos Part a Appl Sci Manuf*. Dec. 2018;115:57-65.
17. İnal O, Balıkoğlu F, Ataş A. Bolted joints in quasi-unidirectional glass-fibre NCF composite laminates. *Compos Struct*. Jan. 2018;183(1): 536-544.
18. Shipsha A, Burman M. Failure mechanisms in NCF composite bolted joints: experiments and FE model. *Compos Part B Eng*. Jul. 2020; 192:107950.
19. Shipsha A, Hallström S, Burman M. Effect of stacking sequence and bundle waviness in quasi-isotropic NCF composites subjected to compression. *Compos Part B Eng*. Dec. 2019;178:107423.
20. Wilhelmsson D, Gutkin R, Edgren F, Asp LE. An experimental study of fibre waviness and its effects on compressive properties of unidirectional NCF composites. *Compos Part a Appl Sci Manuf*. Apr. 2018;107:665-674.
21. Edgren F, Asp LE, Joffe R. Failure of NCF composites subjected to combined compression and shear loading. *Compos. Sci. Technol.* Dec. 2006;66(15):2865-2877.
22. Vallons K, Duque I, Lomov SV, Verpoest I. Loading direction dependence of the tensile stiffness, strength and fatigue life of biaxial carbon/epoxy NCF composites. *Compos Part a Appl Sci Manuf*. Jan. 2011;42(1):16-21.
23. Colin de Verdiere M, Skordos AA, May M, Walton AC. Influence of loading rate on the delamination response of untufted and tufted carbon epoxy non crimp fabric composites: mode I. *Eng Fract Mech*. Dec. 2012;96:11-25.
24. Mei M, He Y, Yang X, Wei K, Qu Z, Fang D. Shear deformation characteristics and defect evolution of the biaxial ±45° and 0/90° glass non-crimp fabrics. *Compos. Sci. Technol.* Jun. 2020;193:108137.
25. Li L, Zhao Y, Vuong H, Chen Y, Yang J, Duan Y. In-plane shear investigation of biaxial carbon non-crimp fabrics with experimental tests and finite element modeling. *Maternite*. Nov. 2014;63:757-765.
26. Arteiro A, Catalanotti G, Xavier J, Camanho PP. Notched response of non-crimp fabric thin-ply laminates. *Compos Sci Technol*. Apr. 2013;79:97-114.
27. Vallons K, Behaeghe A, Lomov SV, Verpoest I. Impact and post-impact properties of a carbon fibre non-crimp fabric and a twill weave composite. *Compos Part a Appl Sci Manuf*. Aug. 2010;41(8):1019-1026.
28. Zhang C, Rao Y, Li Z, Li W. Low-velocity impact behavior of interlayer/intralayer hybrid composites based on carbon and glass non-crimp fabric. *Materials (Basel)*. Dec. 2018;11(12):2472.
29. Zhang C, Rao Y, Li W. Low-velocity impact behavior of intralayer hybrid composites based on carbon and glass non-crimp fabric. *Compos Struct*. Feb. 2020;234:111713.
30. Kaya G. Comparison of the impact damage resistance of non-hybrid and intra-ply hybrid carbon/E-glass/polypropylene non-crimp thermoplastic composites. *J Reinf Plast Compos*. Jan. 2019;38(1):31-45.
31. Zhou F, Zhang J, Song S, Yang D, Wang C. Effect of temperature on material properties of carbon fibre reinforced polymer (CFRP) tendons: experiments and model assessment. *Materials*. 2019;12(7):1025.
32. Kodur VKR, Bisby LA, Foo SHC. Thermal behavior of fire-exposed concrete slabs reinforced with fibre -reinforced polymer bars. *ACI Struct J*. Nov. 2005;102(6):799-807.
33. Bootle J, Burzesi F, Fiorini L. Design guidelines. In: Miracle DB, Donaldson SL, eds. *Composites*. Vol.21. ASM International; 2001.
34. Wang K, Young B, Smith ST. Mechanical properties of pultruded carbon fibre-reinforced polymer (CFRP) plates at elevated temperatures. *Eng Struct*. Jul. 2011;33(7):2154-2161.
35. Yu B, Kodur V. Effect of temperature on strength and stiffness properties of near-surface mounted FRP reinforcement. *Compos Part B Eng*. Mar. 2014;58:510-517.
36. Jia Z, Li T, Chiang F, Wang L. An experimental investigation of the temperature effect on the mechanics of carbon fibre reinforced polymer composites. *Compos. Sci. Technol.* Jan. 2018;154:53-63.

How to cite this article: Lepore MA, Ferrante L, Sanguigno L, Maligno AR. A non-crimp fabric mechanical characterization for the production of aerospace components. *Mat Design Process Comm*. 2021;3(5):e222. https://doi.org/10.1002/mdp2.222